

TP2O: Creative Text Pair-to-Object Generation using Balance Swap-Sampling

Jun Li, Zedong Zhang, and Jian Yang

School of Computer Science and Engineering,
Nanjing University of Science and Technology, Nanjing, China
{junli, zandyz, csjyang}@njjust.edu.cn

<https://tp2o.github.io/anon/>

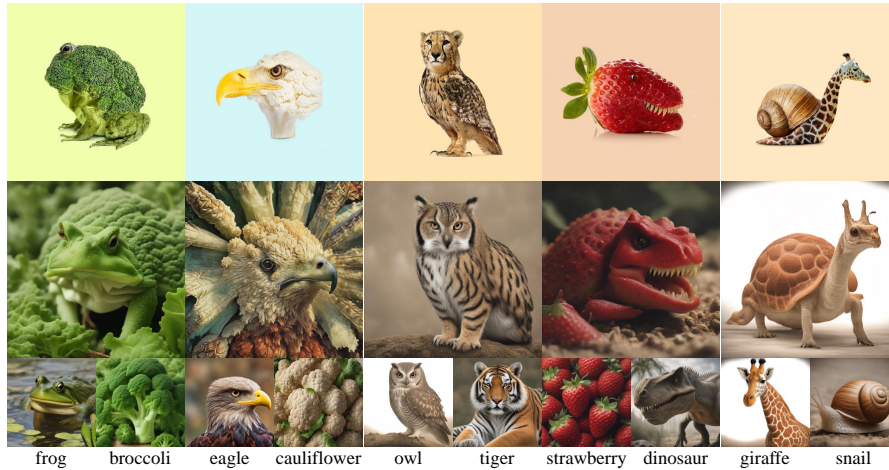


Fig. 1: We propose a simple yet effective sampling method without any training to generate creative combinations from two object texts. Bottom row: original images from Stable-Diffusion2 [46]. Middle row: combinations produced by our algorithm. Top row: artworks by *Les Créatonautes*, a French creative agency. Remarkably, the objects we create rival the artistry of masterpieces crafted by artists.

Abstract. Generating creative combinatorial objects from two seemingly unrelated object texts is a challenging task in text-to-image synthesis, often hindered by a focus on emulating existing data distributions. In this paper, we develop a straightforward yet highly effective method, called **balance swap-sampling**. First, we propose a swapping mechanism that generates a novel combinatorial object image set by randomly exchanging intrinsic elements of two text embeddings through a cutting-edge diffusion model. Second, we introduce a balance swapping region to efficiently sample a small subset from the newly generated image set by balancing CLIP distances between the new images and their original generations, increasing the likelihood of accepting the high-quality combinations. Last, we employ a segmentation method to compare CLIP distances among the segmented components, ultimately selecting the most promising object from the sampled subset. Extensive experiments demonstrate that our approach outperforms recent SOTA T2I methods. Surprisingly, our results even rival those of human artists, such as *frog-broccoli* (see Figures 1).

Keywords: Combinatorial Creativity · Diffusion Model · Text-to-Image
· Balance Swap-Sampling · Human Artworks

1 Introduction

Human creativity plays a crucial role in the innovative visual generation from textual concepts, known as text-to-image (T2I) synthesis, due to its the ability to come up with visual generations that are novel, surprising and valuable [3], such as the combinatorial artworks created by artists in the top of Figure 1. However, this task poses a significant challenge for most existing methods in computer vision, including DALLE3 [44], Stable-Diffusion2 [46], and ERNIE-ViLG2 [18]. These methods aim to generate images that emulate a given training distribution [16], but they often lack the potential for the creativity [12]. Consequently, there is a need to develop a vision system with enhanced creative capabilities.

Recent efforts have primarily focused on compositional objects, aiming to directly generate new and intricate images by composing textual descriptions of multiple known objects. For example, Composable Diffusion Models (CDMs) [37] generates images containing multiple objects at specified positions, and Custom-Diffusion [32] enables the generation of new and reasonable compositions of multi-objects in previously unseen contexts. However, these methods only produce generations with independent objects, lacking the element of combinatorial creativity (see Fig. 1 [17] and Fig. 1 [32]). This raises an interesting task, *Creative Text Pair-to-Object Generation*: produce a creative object using an object text pair, akin to the human artworks using *frog-broccoli* and *turtle-cat*.

To address this question, we adhere to three essential criteria, *novelty*, *surprise* and *value* [3, 38], for evaluating the creativity of the combinatorial object in the T2I synthesis. Creative combinations often lies in their unpredictability for several reasons. Firstly, these three criteria encompass diverse interpretations, including ‘psychological’ and ‘historical’ novelties, along with unfamiliar, unaware and impossible surprises [3]. Moreover, values, particularly in the realm of science, can be elusive and subject to change [3]. Secondly, when combinations become predictable, the element of surprise diminishes as they inherently contain less information entropy. Since T2I models typically rely on datasets with similar distributions, we revisit these criteria when combining two object texts. ***Balanced novelty*** quantifies a balance degree between the two object texts, ensuring that the combined object diverges from both. ***Associated surprise*** measures the improbable association between the two object texts, while ***human-preference value*** assesses the human appeal of the combined object.

Based on the aforementioned criteria, we propose a novel technique called ***Balance Swap-Sampling*** (BASS) that generates combinatorially creative objects by fusing the prompt embeddings of two object concepts. Our approach comprises a text encoder, a swapping mechanism, an image generator, and a balance region using a CLIP metric [43]. To begin, the text encoder and image generator can be pretrained using state-of-the-art T2I models, such as Stable-Diffusion2 [46], and we select impossibly associated categories to form text concept pairs from the

ImageNet [48] for implementing their possibly **surprising** combinations. Initially, we obtain two original embeddings by inputting the prompts of object text pairs into the text encoder, respectively. Then, two original images are generated by using these embeddings in the image generator. Next, we propose a swapping mechanism that interchange intrinsic elements of the prompt embeddings, allowing the image generator to create *novel* combinations. Furthermore, we establish a *balance sampling* region within which the newly created image likely exhibits a high-quality fusion of the two original concepts. This is achieved by carefully managing the CLIP distances between the newly creations and the two originally generations. The balance region allows us to efficiently sample a small subset of the newly created images from a pool of randomly exchanging column vectors. Lastly, we further balance the internal components by employing Segment Anything Model (SAM) [30] to compare the CLIP distances among the segmented components, ultimately selecting the most promising combinatorial image from the sampled subset. Surprisingly, when we utilize PickScore [31] and HPSv2 [56], both trained with human preference datasets, instead of our sampling process, Table 2 reveals that our approach, despite lacking specific training and human preference feedback, still exhibits comparable performance to these models. This underscores that our combined objects hold significant *value* in terms of human preference. Overall, our contributions are summarized as follows:

- We explore a balance swap-sampling approach to produce novel and surprising combinatorial objects without any training, based solely on two object texts. To the best of our knowledge, we are the pioneers in developing a visual system with creative combination capabilities in text-to-image synthesis.
- Our approach involves swapping intrinsic elements within prompt embeddings to generate novel combinations, while controlling CLIP distances between the resulting combination image and the original images to ensure balance for better founding their valuable combination.
- Experimental results demonstrate the effectiveness of our approach in generating previously unseen and creative object images in Figures 1 and 5. Our method surpasses the object images generated by the SOTA T2I techniques.

2 Related Work

Here we mainly review compositional T2I, creativity, and OOD generation.

Text-to-image (T2I) synthesis has garnered increasing attention in recent years due to its remarkable progress [34, 59, 64]. Notably, diffusion models [26, 27, 36, 53, 61] combined with CLIP models [43] have shown great promise in T2I synthesis. For instance, CLIPDraw [19] employs only the CLIP embedding to generate sketch drawings. DALLE2 [44] introduces a diffusion decoder to generate images based on text concepts. Stable-Diffusion [46] has emerged as the most popular choice due to its open-source nature and ability to save inference time.

Compositional T2I primarily focuses on generating new and complex images by combining multiple known concepts. These concepts can be composed in various ways, including object-object, object-color and shape, object conjunction

and negations, object relations, attributes, and modifying sentences by words. Some notable approaches in this field include object-object compositions [17, 32, 37], image-concept compositions such as subject-context, segmentation-text, and sketch-sentence [1, 6, 8, 10, 15, 20, 23, 33, 37, 41, 42, 47]. However, a common limitation of these compositional T2I models is that they often generate images based solely on the compositional text descriptions, which restricts their creativity. Moreover, the existing object-object composition approaches [17, 32, 37] tend to produce images with independent objects. Recent Magicmix [35] closely related to ours employs linear interpolation to merge distinct semantic images and text, aiming to produce novel conceptual images. But the outcomes may sometimes exhibit an unnatural blend and lack artistic value. In contrast, we propose an innovative sampling method that enables effective information exchange between two object concepts, leading to the creation of captivating composite images.

Creativity encompasses the ability to generate ideas or artifacts across various domains, including concepts, compositions, scientific theories, cookery recipes, and more [2, 3, 7, 25, 38, 55]. Recently, there has been significant research exploring the integration of creativity into GANs [21, 22] and VAEs [29]. For instance, CAN [16] extend the capabilities of GANs to produce artistic images by maximizing deviations from established styles while minimizing deviations from the art distribution. CreativeGAN, systematically modifies GAN models to synthesize novel engineering designs [39, 40]. Additionally, CreativeDecoder [9, 11] enhances the decoder of VAEs by utilizing sampling, clustering, and selection strategies to capture neuronal activation patterns. Recent works [4, 5] design a method to assess one-shot generative models in approximating human-produced data by examining the trade-off between *recognizability* and *diversity* (measured by standard deviation). Unlike these methods, our approach introduces a swapping mechanism to enhance the generation of novel combinational object images, along with a defined region for accepting high-quality combinations.

Out-of-Distribution (OOD) is closely related to our work as we generate creative object images that lie outside the data distribution. However, existing OOD techniques primarily concentrate on detection tasks [52, 58] through disentangled representation learning [54], causal representation learning [28, 51], domain generalization [62, 63], and stable learning [57]. In contrast, our focus is on OOD generation, where we aim to create meaningful object images. While [45] also incorporate an OOD generation step for the OOD detection task, they primarily address scenarios where the input distribution has shifted. To augment the limited dataset for the image classification task, diffusion models are employed to produce numerous images through outlier [14] and guidance [60] imaginations within the same category. In our approach, we create a novel distribution by blending the embedding distributions of two category concepts.

3 Methodology

In this section, we introduce a balance swap-sampling (BASS) approach for generating a new and surprising object using two text concepts, as shown in

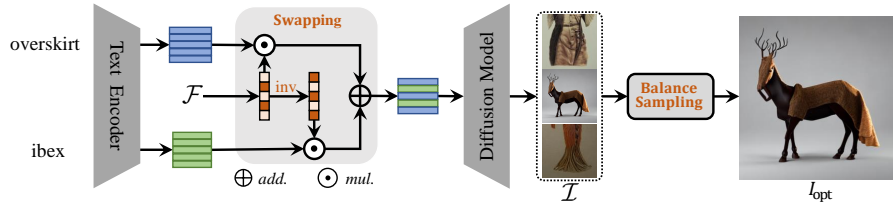


Fig. 2: The pipeline of our balance swap-sampling method. Starting from text embeddings by inputting two given texts into the text encoder, we introduce a swapping operation to collect a set \mathcal{F} of randomly swapping vectors for novel embeddings, then generate a new image set \mathcal{I} , and propose a balance region to build a sampling method for selecting an optimal combinatorial object image.

Figure 2. Its key parts include a swapping mechanism, a balance region and Our BASS method. Before showing the details of our method, we provide an overview of the unified generation process using the T2I models (e.g., Stable-Diffusion2 [46], DALLE2 [44], and Imagic [49]).

T2I: For a text t and its associated prompt p , a generated image is described as $G = \mathcal{G}(E)$, where $E = \mathcal{E}(p) \in \mathbb{R}^{h \times w}$ is a text encoder with dimensions h and w , and $\mathcal{G}(\cdot) \in \mathbb{R}^{H \times W}$ is an image generator with dimensions H and W . The variable h denotes the maximum number of input words, while w represents the dimensionality of each word embedding. H and W denote the size of the generated image. Note that the text encoder $\mathcal{E}(\cdot)$ and the image generator $\mathcal{G}(\cdot)$ can be pretrained using Stable-Diffusion2 [46], as our baseline. Alternatively, any other diffusion model can also be utilized in our approach.

Given a text pair (t_1, t_2) , we use the T2I model to generate their original images $I_1 = \mathcal{G}(\mathcal{E}(p_1))$ and $I_2 = \mathcal{G}(\mathcal{E}(p_2))$, where p_1 and p_2 are the prompts of t_1 and t_2 , respectively. For example, for a text pair (*frog*, *broccoli*), we use its prompt pair (*A photo of frog*, *A photo of broccoli*), to produce two images, please refer to the two below figures in the first column of the Figure 1.

3.1 Swapping Mechanism

Following the generation process of the T2I model, we propose a swapping operation to mix well the prompt embeddings of a prompt pair for a novel object image generation, as shown in the left part of Figure 2. The swapping process is formalized as the following three steps:

- **Encoding** a prompt pair (p_1, p_2) by using a text encoder,

$$E_1 = \mathcal{E}(p_1) \in \mathbb{R}^{h \times w} \quad \text{and} \quad E_2 = \mathcal{E}(p_2) \in \mathbb{R}^{h \times w}, \quad (1)$$

- **Swapping** their intrinsic elements by using an exchanging vector $f \in \{0, 1\}^{w \times 1}$,

$$E_f = E_1 \text{diag}(f) + E_2 \text{diag}(1 - f) \in \mathbb{R}^{h \times w}, \quad (2)$$



Fig. 3: Visualization comparison of different swapping ways.

- **Generating** a novel image by using an image generator,

$$I_f = \mathcal{G}(E_f) \in \mathbb{R}^{H \times W}, \quad (3)$$

where $\text{diag}(\cdot)$ is an operation to diagonalize a vector, and $f \in \{0, 1\}^{w \times 1}$ is a binary vector to swap the column vectors of the prompt embeddings E_1 and E_2 . (Neural swapping process, please see the *Supp. Mat. A*.)

Discussions on swapping ways between E_1 and E_2 . Here, we discuss four swapping ways to ingeniously merge the meaningful characteristics of these prompt embeddings, as shown in Figure 3. The first way is a simple and popular *linear interpolation*, spanning a linear embedding space using $\alpha E_1 + (1 - \alpha) E_2$, where α ranges from 0 to 1. Nevertheless, since this method mixes the whole embedding manifolds, it may struggle to blend the inherent characteristics of the embeddings E_1 and E_2 effectively, often resulting in predictable and unremarkable outcomes. The second way *swaps the row vectors* of these embeddings, corresponding to words (objects). Similarly, it faces challenges in effectively exchanging intrinsic elements. To achieve a more surprising combination, the third way *swaps all the corresponding elements* of E_1 and E_2 . However, the computational cost of finding the swapping matrix makes it impractical. In contrast, the fourth way *swaps the column vectors* of these embeddings, effectively mixing the inherent characteristics of the words. This increases the likelihood of creative combinations. Several experiments have demonstrated meaningful results by swapping the column vectors multiple times, as shown in Figures 1 and 5.

3.2 Balance Region

Using the above swapping technique in the Equations (1)-(3), a new image I_f is created by combining the text prompts p_1 and p_2 . In this subsection, we establish a balance region to sample potentially high-quality combinations depending on only the images (I_1 and I_2) generated using p_1 and p_2 as anchor points, excluding human priors. This region adheres to a fundamental sense:

A new image I_f can be considered of potentially high-quality combination if it maintains an appropriate balance in distance from the anchor images I_1 and I_2 .

This distance must adhere to three key rules. The first rule entails maintaining a balance between the distances from I_f to I_1 and from I_f to I_2 , demonstrating an equilibrium between them. The second rule highlights that a substantial separation between these distances signals a higher likelihood of generating content that is disordered, devoid of meaningful. The third rule underscores that a minimal distance indicates that the generated image closely resembles the input data, potentially lacking novelty and surprise. In mathematical terms, we can formalize them into two distance criteria:

- **Balancing Distances:** Achieving a balance between the distances $d(I_f, I_1)$ and $d(I_f, I_2)$ through an inequality involving a constant α ,

$$|d(I_f, I_1) - d(I_f, I_2)| \leq \alpha, \quad (4)$$

- **Controlling Bounds:** Constraining the upper bound of the average distance between $d(I_f, I_1)$ and $d(I_f, I_2)$ by using an inequality with a constant β ,

$$d(I_f, I_1) + d(I_f, I_2) \leq 2\beta, \quad (5)$$

where $\alpha \geq 0$, $\beta \geq d(I_1, I_2)/2 \geq 0$, $d(I_1, I_2)$ is the distance between the anchor images I_1 and I_2 , $|\cdot|$ is the absolute value function, and $d(a, b) \geq 0$ is a positive function to compute the distance between a and b . These two criteria govern a region in within which the combinatorial image I_f has the potential to be potential high-quality. Now, let’s delve into a geometrical analysis.

Geometrical Explanations. In defining the potential combinatorial space for image I_f , we employ geometric shapes—a hyperbola and an ellipse—as shown in Figure 4. The hyperbola constrains combinatorial images per Equation (4): $|d(I_f, I_1) - d(I_f, I_2)| = \alpha$, where α is constant and I_1 and I_2 are fixed points, delineating the grey-shaded area. At $\alpha = 0$, it forms a balanced perpendicular line between I_1 and I_2 . Similarly, Equation (5) defines an elliptical upper boundary: $(d(I_f, I_1) + d(I_f, I_2)) = 2\beta$, with I_1 and I_2 fixed and β constant, representing blue-shaded areas. At $\beta = d(I_1, I_2)/2$, it creates a line between I_1 and I_2 . Considering both shapes simultaneously, I_f falls within the overlapping orange region, indicating potential for high-quality blended images. Acceptable and rejected images are represented by circle and fork points, respectively.

While the balance region is not flawless, it offers control over I_f quality to a degree in Figure 4. Additionally, green areas depict distributions of original

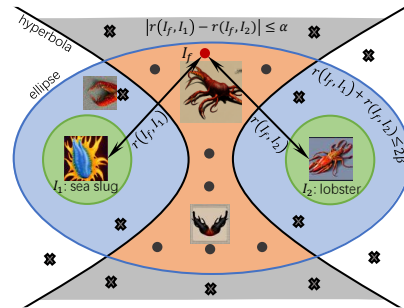


Fig. 4: Geometrical visualization of the high-quality composite image’s potential orange region by balancing the distances between I_f and the anchor images I_1 , I_2 .

images I_1 and I_2 , contrasting with the orange region. This diagram shows that images within our balance region deviate from the data distribution, as evidenced by comparison with dataset retrievals in Figure 5.

3.3 Balance Swap-Sampling

By combining the swapping technique with the balance region, we propose a balance swap-sampling method to sample a promising blend image I_f on the prompt pair (p_1, p_2) . We first generate a set of N randomly swapping vectors \mathcal{F} , and correspondingly produce an image set \mathcal{I} using the Equations (1)-(3). Note that $f \in \mathcal{F}$ corresponds to $I_f \in \mathcal{I}$ one by one. Depending on the prompts p_1, p_2 , and their generated images I_1, I_2 , we introduce a coarse-to-fine sampling process comprising the following three steps.

Coarse Sampling Using Semantic Distance. We select a coarse subset $\mathcal{I}_{\text{coarse}}$ from the set \mathcal{I} by using a semantic balance, similar to the Equation (4). This helps us maintain a balanced semantic content between the image I_f and the text prompts p_1 and p_2 . The coarse sampling is defined as:

$$\mathcal{I}_{\text{coarse}} = \{I_f \mid |d(I_f, p_1) - d(I_f, p_2)| \leq \theta, \quad I_f \in \mathcal{I}\}, \quad (6)$$

where θ is a width threshold of the semantic balance area. Here, we fix θ at 0.05.

Fine Sampling Using Image Distances. We further choose a fine subset $\mathcal{I}_{\text{fine}}$ from $\mathcal{I}_{\text{coarse}}$ by using the balance region in the Equations (4) and (5), ensuring a balanced relationship among I_f, I_1 and I_2 . This leads to potential high-quality combinations. The fine sampling is expressed as:

$$\mathcal{I}_{\text{fine}} = \{I_f \mid |d(I_f, I_1) - d(I_f, I_2)| \leq \alpha \ \& \ d(I_f, I_1) + d(I_f, I_2) \leq 2\beta, \quad I_f \in \mathcal{I}_{\text{coarse}}\}. \quad (7)$$

where $\alpha = d_{\lceil |\mathcal{I}_{\text{coarse}}| \cdot \bar{\alpha} \rceil}^d$, $\beta = d_{\lceil |\mathcal{I}_{\text{coarse}}| \cdot \bar{\beta} \rceil}^s$, $0 \leq \bar{\alpha} \leq 1$, $0 \leq \bar{\beta} \leq 1$, $\lceil \cdot \rceil$ denotes rounding up to the nearest integer, $|\mathcal{I}_{\text{coarse}}|$ represents the cardinality of the set $\mathcal{I}_{\text{coarse}}$, and d_i^d and d_i^s refer to the i -th element of the descendingly sorted sets $\mathcal{D}^d = \{d^d = |d(I_f, I_1) - d(I_f, I_2)|, I_f \in \mathcal{I}_{\text{coarse}}\}$ and $\mathcal{D}^s = \{d^s = d(I_f, I_1) + d(I_f, I_2), I_f \in \mathcal{I}_{\text{coarse}}\}$, respectively. In this paper, we set $\bar{\alpha} = 0.4$, and $\bar{\beta} = 0.1$. The subset $\mathcal{I}_{\text{fine}}$ indicates images that may exhibit excellent mixing characteristics, denoted as black points within the orange region in Figure 4.

Choosing the Optimal Image Using Segmentation Methods. Unfortunately, $\mathcal{I}_{\text{fine}}$ is not directly employed for the ideal selection. Instead, we adopt the Segment Anything Model (SAM) [30] to enhance the visual semantic components, thereby facilitating the selection of the optimal combinatorial image. The final selection is made by maximizing the following objective:

$$I_{\text{opt}}^{(p_1, p_2)} = \arg \max_{I_f \in \mathcal{I}_{\text{fine}}} \{r(I_f, I_1, I_2)\} \quad \text{with} \\ r(I_f, I_1, I_2) = (s(I_f, I_1) + s(I_f, I_2)) / 2, \quad (8)$$

Algorithm 1 Balance Swap-Sampling (BASS).

-
- 1: **input:** prompt pair (p_1, p_2) , their images I_1, I_2 ;
 - 2: **initialize:** $\theta = 0.05, \bar{\alpha} = 0.4, \bar{\beta} = 0.1, N = 200$;
 - 3: Generate a set \mathcal{F} of N randomly swapping vectors;
 - 4: Produce an image set \mathcal{I} using Eqs. (1)-(3) and $f \in \mathcal{F}$;
 - 5: Sample a coarse subset $\mathcal{I}_{\text{coarse}}$ from \mathcal{I} by Eq. (6) with θ ;
 - 6: Sample a fine subset $\mathcal{I}_{\text{fine}}$ from $\mathcal{I}_{\text{coarse}}$ by Eq. (7) with $\bar{\alpha}, \bar{\beta}$;
 - 7: Choose the optimal image $I_{\text{opt}}^{(p_1, p_2)}$ from $\mathcal{I}_{\text{fine}}$ by Eq. (8);
 - 8: **output:** $I_{\text{opt}}^{(p_1, p_2)}$.
-

where $s(I_f, I_i) = \frac{1}{|\mathcal{C}_i| \times |\mathcal{C}_f|} \sum_{c_f \in \mathcal{C}_f, c_i \in \mathcal{C}_i} d(c_f, c_i)$, $\mathcal{C}_i = \text{SAM}(I_i) (i = 1, 2)$, $\mathcal{C}_f = \text{SAM}(I_f)$, and $\text{SAM}(I)$ represents a collection of segmented components extracted from the image I using SAM [30]. Using Equation (8), we identify the optimal image from the $\mathcal{I}_{\text{fine}}$, as depicted by red points in Figure 4. This process culminates in the creation of a combinatorial object image that is both promising and amazing. Overall, our BASS is outlined in **Algorithm 1**. Note that we define the distance function as $d(a, b) = \cos(\phi(a), \phi(b))$, where $\cos(\cdot, \cdot)$ represents a cosine similarity, and $\phi(\cdot)$ corresponds to the features using the CLIP model [43].

4 Experiments

4.1 Experimental Settings

Dataset. To showcase the power of combinational creativity in T2I synthesis, we have curated a novel dataset comprising prompt pairs. We leveraged the vast vocabulary of ImageNet [48], consisting of 1,000 categories, to form our text set. From this collection, we randomly selected two distinct words to construct each prompt pair, such as *macaque-timber wolf*. Our dataset encompasses a total of 5075 prompt pairs, representing a fraction of the possible combinations. In addition, to compare the human artworks, we have gathered a selection of pieces created by *Les Créatonautes* from the Instagram¹.

Sampling Settings. For the sampling process, the text encoder $\mathcal{E}(\cdot)$ and the image generator $\mathcal{G}(\cdot)$ were pretrained using the CLIP model with ViT-L/14@336p backbone [43] and Stable-Diffusion2 [46] or Stable-Diffusion XL turbo², respectively. This CLIP model [43] was also employed in the distance function. The Segment Anything Model (SAM) [30] served as the pre-trained segmentation method. We conducted our experiments using four NVIDIA GeForce RTX 3090 GPUs, with a batch size of 64 per GPU.

Evaluation metrics. Following the creative criteria, we evaluate the combinatorial object images generated by our method as follow. Firstly, we denote the cosine similarity between a and b using the CLIP model as $\text{cos}(a, b)$. From the

¹ <https://www.instagram.com/les.creatonautes/>

² <https://clipdrop.co/stable-diffusion-turbo>



Fig. 5: Visual comparisons of combinatorial object generations. We compare our BASS with Stable-Diffusion2 [46], DALLE2 [44], ERNIE-ViLG2 (Baidu) [18] and Bing (Microsoft) using a hybrid prompt. For a fairer comparison, we incorporate detailed textual descriptions alongside our generated images as input prompts. However, these models have not achieved results closely aligned with our own, highlighting the superior creative combinatorial capabilities of our BASS. Furthermore, our results notably differ from images retrieved from the LAION-5B dataset [50] in the first row, highlighting our model’s capacity to produce out-of-distribution images.

generated image I_f and the prompt pairs (p_1, p_2) with their corresponding images (I_1, I_2) , we define text- and image-balance metrics as $|\cos(I_f, p_1) - \cos(I_f, p_2)|$ and $|\cos(I_f, I_1) - \cos(I_f, I_2)|$, respectively, to quantify the degree of balance. Smaller metrics indicate better balance. Additionally, we define text- and image-average similarities as $(\cos(I_f, p_1) + \cos(I_f, p_2))/2$ and $(\cos(I_f, I_1) + \cos(I_f, I_2))/2$, respectively, to measure novelty. Smaller similarities indicate higher novelty. Secondly, we randomly select two distinct categories from ImageNet [48] to create *surprising* prompt pairs. Thirdly, we employ PickScore [31] and HPS-v2 [56], which fine-tuned their CLIP models using human-preference datasets, to evaluate their *human-preference values*. Finally, we also conduct a user study to assess the creativity of our combinatorial objects.

4.2 Main Results

We conducted a comprehensive comparison of our BASS method with some human artworks created by *Les Créatonautes*, four prominent Text-to-Image (T2I) models (i.e., Stable-Diffusion2 [46], DALLE2 [44], ERNIE-ViLG2 [18] and Bing), and one combinational method, (i.e., Magicmix [35], which bears the closest relevance to our work). Note that as Magicmix currently does not offer an available software, we utilized its unofficial implementation [13].

Comparison with Artworks Created by Human Artists. Figure 1 presents both human artworks (top row) and our creations (middle row) across corresponding category pairs. Surprisingly, our BASS exhibits the remarkable ability to generate novel and astonishing species unprecedented in reality, contrasting with the seemingly natural assembly in human artworks. For example, the fusion of an owl with the distinctive features of a tiger in our creation *owl-tiger* showcases a blend of owl attributes with the texture, feet, and eye of a tiger, while the human artwork merely substitutes the tiger’s head for that of an owl. Unlike the human depiction of *giraffe-snail*, which maintains the snail’s shell and substitutes its body with that of a giraffe, our result uniquely features a snail adorned with the giraffe’s head and legs, as depicted in Figure 1. Furthermore, we enlisted the opinions of 116 non-artists to evaluate eight artworks alongside our creations. From this study, we amassed a total of 928 votes, with 71.3% of non-artists expressing a preference for our creations. For additional comparisons and detailed information on the non-artists study, please refer to *Supp. Mat. B*.

Comparison with the SOTA T2I models. Figure 5 showcase several examples of image generation achieved through those models using prompt pairs. We make the following three observations. First, compared to the SOTA T2I models, our BASS exhibits a stronger ability to generate a creative object by inputting two different objects. Although the images generated by other models are colorful and rich in detail, they do not fully display the mixed features of the two objects, as seen in *macaque-timber wolf* and *zucchini-vulture* in Figure 5. Second, to evaluate the Out-Of-Distribution (OOD) generation ability of our BASS, we conducted a retrieval on the entire LAION-5B dataset [50] to find the most similar image in the first row of Figure 5. By comparing our created images with the retrieved images, we found that they significantly differ from the retrieved ones, highlighting the distinctiveness of our BASS’s output. Note that our BASS generation differs from outlier [14] and guidance [60] imaginations as they generate the data in the same category. Third, when comparing the images generated using intricate textual descriptions in conjunction with our created images as input prompts, these models still struggles to create plausible compositions, such as *A timber wolf with a macaque face* in the Figure 5. While Bing employs *A vulture with the texture of zucchini on its wings* to generate an object that looks beautiful, it utilizes entire zucchinis as the vulture’s wings, rather than utilizing their texture. More results, refer to *Supp. Mat. G*.

Comparison with Magicmix. As Magicmix [35] works with image-text inputs, our BASS utilizes both the image category and accompanying text to create a text pair. Figure 6 shows the resulting combinational object images,

observing that our BASS excels in seamlessly blending the features of both tiger and rabbit, incorporating elements like the rabbit’s ears and the tiger’s face more naturally. In contrast, Magicmix merely overlays the tiger’s texture onto the rabbit, resulting in an unnatural appearance. More results, refer to *Supp. Mat. C*.

Evaluating novelty, surprise and value. Since we randomly choose two distinct categories from ImageNet [48] to form text pairs, creating seemingly impossible associations, this selection directly confirms the *associated surprise* of potential combinations, such as *zucchini-vulture*, *frog-broccoli*, and *monarch-cheetah*. Our focus here is on assessing novelty and value.

Balanced novelty. Table 1 reports the metrics for text- and image-balance, as well as text- and image-average similarities. Our observations are as follows:

1) Our BASS exhibits superior balance compared to MagicMix [35]. 2) Both BASS and MagicMix demonstrate lower similarity, evidenced by values lower than the similarity between the text prompt and its generated image, which consistently approaches 1. 3) While MagicMix slightly outperforms our BASS in novelty, its visual outputs, in Figure 6, are less intuitive than ours.

Human-preference value. To assess the human-like superiority of our BASS method, we employed PickScore [31] and HPSv2 [56] to calculate evaluation scores for selecting the optimal image with the highest score from the new image set \mathcal{I} . Subsequently, we utilized these metrics to evaluate the optimal images, and the findings are presented in Table 2. Our results indicate that our BASS method closely rivals the performance of PickScore and HPSv2. Notably, our method operates independently of human intervention, except for the selection of hyper-parameters using HPSv2. In contrast, both PickScore and HPSv2 rely on human-preference datasets to fine-tune the CLIP models for T2I model evaluation. This demonstrates our BASS possesses a capability with *comparable human-preference value*. Furthermore, the

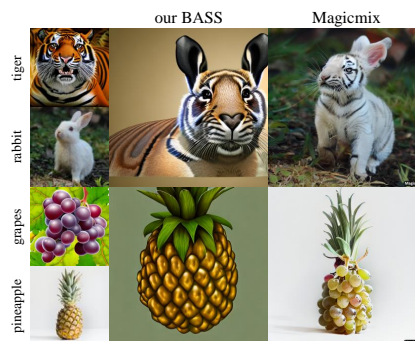


Fig. 6: Combinational comparison.

Table 1: Quantitative comparisons.

Model	Score	text-		image-	
		avg. sim.↓	balance↓	avg. sim.↓	balance↓
our BASS		0.328	0.061	0.543	0.126
MagicMix [35]		0.282	0.100	0.536	0.220



Fig. 7: Sampling visualizations compared our BASS with HPSv2 and PickScore.

sampling examples are illustrated in Figure 7. Our BASS method excels in generating superior combinatorial images compared to both HPSv2 and PickScore.

Table 2: Quantitative comparisons. **Table 3:** User study of combinatorial creations.

Models	PickScore [31]	HPSv2 [56]	Our BASS
PickScore \uparrow	0.207	0.202	0.200
HPSv2 \uparrow	0.246	0.253	0.242

Models	Our BASS	SD2 [46] (baseline)	DALLE2 [44]	ERNIE-ViLG2 [18]	Bing
Vote \uparrow	658	98	59	49	196

User Study. We conducted a user study to assess the combinatorial creativity of our model against four other T2I methods in Table 3 and *Supp. Mat. D*. Each user evaluated 10 prompt pairs, resulting in 1,060 votes from 106 users. Our model garnered the highest number of votes, with 62% of users favoring its creative outputs. The Bing model attracted interest from 18.5% of users, while DALLE2 [44] received only 5% of the votes despite its structural similarities to the Bing model. Stable-Diffusion2 [46] received 9% of the votes, while ERNIE-ViLG2 [18] was preferred by only 4.6% of users.

Computational Costs. In contrast to the baseline (Stable-Diffusion2), our additional models include CLIP and SAM. For a single text pair, we parallelize the data to complete the inter-evaluation process in 10 minutes using 4 RTX 4090 GPUs. *When using Stable-Diffusion XL turbo in the same setting, it only requires a mere 40 seconds to discover meaningful object images.*

4.3 Parameter Analysis and Ablation Study.

Parameter Analysis. During the sampling process, we determined the parameters θ in the Equation (6), and $\bar{\alpha}$, and $\bar{\beta}$ in the Equation (7) using 20 text pairs. To begin, for each prompt pair (p_1, p_2) , we produce an image set \mathcal{I} by randomly generating a set \mathcal{F} consisting of $N = 200$ swapping vectors. From \mathcal{I} , we coarsely select a subset $\mathcal{I}_{\text{coarse}}$ using Equation (6), and the parameter θ is set to 0.05 by choosing the best

Table 4: Parameter analysis with θ using average HPSv2 scores [56] of 20 text pairs. $+\infty$ represents all sampling images.

θ	0.01	0.02	0.05	0.1	$+\infty$
HPSv2	0.2444	0.2451	0.2458	0.2392	0.2361

Table 5: Parameter analysis with $\bar{\alpha}$ and $\bar{\beta}$ using average HPSv2 scores [56] of 20 text pairs.

$\bar{\alpha} \setminus \bar{\beta}$	0	0.2	0.4	0.6
0	0.241	0.231	0.230	0.223
0.1	0.231	0.242	0.243	0.239
0.2	0.242	0.230	0.237	0.224
0.3	0.240	0.231	0.235	0.225

average HPSv2 score [56] in Table 4. This reduces the size of $\mathcal{I}_{\text{coarse}}$ approximates to 150. Next, we finely choose a subset $\mathcal{I}_{\text{fine}}$ from $\mathcal{I}_{\text{coarse}}$ using the Equation (7). We set that $\bar{\alpha} = 0.4$ and $\bar{\beta} = 0.1$ by selecting the best average HPSv2 score in Table 5. This reduces the size of $\mathcal{I}_{\text{fine}}$ to around 10. Finally, we obtain the optimal image $I_{\text{opt}}^{(p_1, p_2)}$ by maximizing the problem in the Equation (8). For illustrations of the sampled images using different θ , $\bar{\alpha}$, and $\bar{\beta}$, refer to *Supp. Mat. E*.

Ablation Study of SAM. As SAM [30] is used to enhance the greater similarity in semantic components in semantic components with the original objects I_1 and I_2 within the final sampling set $\mathcal{I}_{\text{fine}}$, we conducted an ablation study to show the effectiveness of SAM in Figure 8. Using SAM, we can choose better combinatorial object images.



Fig. 8: Ablation study of SAM.



Fig. 9: Failure samples in sampling stage.

4.4 Discussions

We mainly discuss the potential applications and limitation of our BASS.

Potential applications. Firstly, we excel at crafting innovative and captivating animated characters for the entertainment and film industry (e.g., *monarch-cheetah* in Figure 5). Secondly, we possess the capability to generate imaginative artworks suitable for art design (e.g., *frog-broccoli* and *turtle-cat* in Figures 1). For example, *Les Créatonautes* designs the visual association between completely different objects³. Thirdly, our method extends the scope of the *Out Of Distribution* (OOD) task to a new generation (see Figure 5). Lastly, we pave the way for translating qualitative descriptions of creativity into achievable technologies within the realm of computer vision.

Limitation. Our method, despite its strengths, has a limitation: the balance-swapping region can sometimes result in non-meaningful or chaotic images. The high-quality balance area in an unsupervised manner continues to pose a challenging problem that necessitates further investigation, as shown in Figure 9. We have included more failure examples in the *Supp. Mat. F* for reference.

5 Conclusion

We have incorporated a simple sampling method into text-to-image synthesis, proposing a balance swap-sampling schema to generate meaningful objects by combining seemingly unrelated object concepts. Our first idea involves a swapping process that exchanges important information from two given prompts, resulting in the creation of fresh object images that go beyond these prompts, even the original data distribution, thereby enhancing novelty. Additionally, we introduce a balance region based on the CLIP metric, which balances the distance among the given prompts, original image generations, and our creations to sample high-quality combinatorial object images from this pool of fresh object images. We further employ the segment anything model to enhance the visual semantic components to select the optimal combinatorial image. Experimental results demonstrate that our approach surpasses popular T2I models in terms of generating creative combinatorial objects, comparable to human artworks designed by *Les Créatonautes*, a French creative agency.

³ <https://www.lescreatonautes.fr/>

References

1. Avrahami, O., Hayes, T., Gafni, O., Gupta, S., Taigman, Y., Parikh, D., Lischinski, D., Fried, O., Yin, X.: Spatext: Spatio-textual representation for controllable image generation. In: Proceedings of the IEEE/CVF Conference on Computer Vision and Pattern Recognition (CVPR). pp. 18370–18380 (2023) [4](#)
2. Boden, M.A.: Creativity and artificial intelligence. *Artificial Intelligence* **103**, 347–356 (1998) [4](#)
3. Boden, M.A.: The creative mind-Myths and mechanisms. Taylor & Francis e-Library (2004) [2](#), [4](#)
4. Boutin, V., Fel, T., Singhal, L., Mukherji, R., Nagaraj, A., Colin, J., Serre, T.: Diffusion models as artists: Are we closing the gap between humans and machines? In: Proceedings of the International Conference on Machine Learning (ICML). pp. 2953–3002 (2023) [4](#)
5. Boutin, V., Singhal, L., Thomas, X., Serre, T.: Diversity vs. recognizability: Human-like generalization in one-shot generative models. In: Proceedings of Advances in Neural Information Processing Systems. pp. 20933–20946 (2022) [4](#)
6. Brooks, T., Holynski, A., Efros, A.A.: Instructpix2pix: Learning to follow image editing instructions. In: Proceedings of the IEEE/CVF Conference on Computer Vision and Pattern Recognition (CVPR). pp. 18392–18402 (2023) [4](#)
7. Cetinic, E., She, J.: Understanding and creating art with ai: Review and outlook. *ACM Trans. Multimedia Comput. Commun. Appl.* **18**(2), Article 66 (2022) [4](#)
8. Chefer, H., Alaluf, Y., Vinker, Y., Wolf, L., Cohen-Or, D.: Attend-and-excite: Attention-based semantic guidance for text-to-image diffusion models. *ACM Trans. Graph.* **42**(4), 148 (2023) [4](#)
9. Cintas, C., Das, P., Quanz, B., Tadesse, G.A., Speakman, S., Chen, P.Y.: Towards creativity characterization of generative models via group-based subset scanning. In: Proceedings of the International Joint Conference on Artificial Intelligence (IJCAI). pp. 4929–4935 (2022) [4](#)
10. Cong, Y., Min, M.R., Li, L.E., Rosenhahn, B., Yang, M.Y.: Attribute-centric compositional text-to-image generation. arXiv:2301.01413 (2023) [4](#)
11. Das, P., Quanz, B., Chen, P.Y., Wook Ahn, J., Shah, D.: Toward a neuro-inspired creative decoder. In: Proceedings of the International Joint Conference on Artificial Intelligence (IJCAI). pp. 2746–2753 (2020) [4](#)
12. Das, P., Varshney, L.R.: Explaining artificial intelligence generation and creativity. *IEEE Signal Processing Magazine* **39**(4), 85–95 (2022) [2](#)
13. daspartho: MagicMix (Jan 2022), <https://github.com/daspartho/MagicMix#magicmix> [11](#), [21](#), [22](#)
14. Du, X., Sun, Y., Zhu, X., Li, Y.: Dream the impossible: Outlier imagination with diffusion models. In: Proceedings of Advances in Neural Information Processing Systems (2023) [4](#), [11](#)
15. Du, Y., Li, S., Mordatch, I.: Compositional visual generation with energy based models. In: Proceedings of the Advances in Neural Information Processing Systems (NeurIPS). p. 6637–6647 (2020) [4](#)
16. Elgammal, A., Liu, B., Elhoseiny, M., Mazzone, M.: Can: Creative adversarial networks: Generating “art” by learning about styles and deviating from style norms. In: International Conference on Computational Creativity (ICCC). pp. 96–103 (2017) [2](#), [4](#)
17. Feng, W., He, X., Fu, T.J., Jampani, V., Akula, A.R., Narayana, P., Basu, S., Wang, X.E., Wang, W.Y.: Training-free structured diffusion guidance for compositional

- text-to-image synthesis. In: Proceedings of the International Conference on Learning Representations (ICLR) (2023) [2](#), [4](#)
18. Feng, Z., Zhang, Z., Yu, X., Fang, Y., Li, L., Chen, X., Lu, Y., Liu, J., Yin, W., Feng, S., Sun, Y., Tian, H., Wu, H., Wang, H.: Ernie-vilg 2.0: Improving text-to-image diffusion model with knowledge-enhanced mixture-of-denoising-experts. In: Proceedings of the IEEE/CVF Conference on Computer Vision and Pattern Recognition (CVPR). pp. 10135–10145 (2023) [2](#), [10](#), [11](#), [13](#), [24](#)
 19. Frans, K., Soros, L.B., Witkowski, O.: Clipdraw: Exploring text-to-drawing synthesis through language-image encoders. In: Proceedings of the Advances in Neural Information Processing Systems (NeurIPS) (2022) [3](#)
 20. Gal, R., Alaluf, Y., Atzmon, Y., Patashnik, O., Bermano, A.H., Chechik, G., Cohen-or, D.: An image is worth one word: Personalizing text-to-image generation using textual inversion. In: Proceedings of the International Conference on Learning Representations (ICLR) (2023) [4](#)
 21. Ge, S., Goswami, V., Zitnick, C.L., Parikh, D.: Creative sketch generation. In: Proceedings of the International Conference on Learning Representations (ICLR) (2021) [4](#)
 22. Goodfellow, I., Pouget-Abadie, J., Mirza, M., Xu, B., Warde-Farley, D., Ozair, S., Courville, A., Bengio, Y.: Generative adversarial nets. In: Proceedings of the Advances in Neural Information Processing Systems (NeurIPS). pp. 2672–2680 (2014) [4](#)
 23. Hertz, A., Mokady, R., Tenenbaum, J., Aberman, K., Pritch, Y., Cohen-Or, D.: Prompt-to-prompt image editing with cross attention control. In: Proceedings of the International Conference on Learning Representations (ICLR) (2023) [4](#)
 24. Hinton, G., Srivastava, N., Swersky, K.: Neural networks for machine learning lecture 6a overview of mini-batch gradient descent. University of Toronto, Course-CSC321 (2012) [20](#)
 25. Hitsuwari, J., Ueda, Y., Yun, W., Nomura, M.: Does human–ai collaboration lead to more creative art? aesthetic evaluation of human-made and ai-generated haiku poetry. *Computers in Human Behavior* **139**(2), 107502 (2023) [4](#)
 26. Ho, J., Jain, A., Abbeel, P.: Denoising diffusion probabilistic models. In: Proceedings of Advances in Neural Information Processing Systems (NeurIPS). pp. 6840–6851 (2020) [3](#)
 27. Kawar, B., Elad, M., Ermon, S., Song, J.: Denoising diffusion restoration models. In: Proceedings of the Advances in Neural Information Processing Systems (NeurIPS) (2022) [3](#)
 28. Khemakhem, I., Kingma, D., Monti, R., Hyvarinen, A.: Variational autoencoders and nonlinear ica: A unifying framework. In: Proceedings of International Conference on Artificial Intelligence and Statistics (AISTATS). pp. 2207–2217 (2020) [4](#)
 29. Kingma, D.P., Welling, M.: Auto-encoding variational bayes. In: Proceedings of the International Conference on Learning Representations (ICLR) (2014) [4](#)
 30. Kirillov, A., Mintun, E., Ravi, N., Mao, H., Rolland, C., Gustafson, L., Xiao, T., Whitehead, S., Berg, A., Lo, W.Y., Dollar, P., Girshick, R.: Segment anything. In: Proceedings of the IEEE International Conference on Computer Vision (ICCV) (2023) [3](#), [8](#), [9](#), [13](#)
 31. Kirstain, Y., Polyak, A., Singer, U., Matiana, S., Penna, J., Levy, O.: Pick-a-pic: An open dataset of user preferences for text-to-image generation. arXiv preprint arXiv:2305.01569 (2023) [3](#), [10](#), [12](#), [13](#)
 32. Kumari, N., Zhang, B., Zhang, R., Shechtman, E., Zhu, J.Y.: Multi-concept customization of text-to-image diffusion. In: Proceedings of the IEEE/CVF Conference on Computer Vision and Pattern Recognition (CVPR). pp. 1931–1941 (2023) [2](#), [4](#)

33. Li, Z., Min, M.R., Li, K., Xu, C.: Stylet2i: Toward compositional and high-fidelity text-to-image synthesis. In: Proceedings of the IEEE/CVF Conference on Computer Vision and Pattern Recognition (CVPR). pp. 18197–18207 (2022) [4](#)
34. Liao, W., Hu, K., Yang, M.Y., Rosenhahn, B.: Text to image generation with semantic-spatial aware gan. In: Proceedings of the IEEE/CVF Conference on Computer Vision and Pattern Recognition (CVPR). pp. 18187–18196 (2022) [3](#)
35. Liew, J.H., Yan, H., Zhou, D., Feng, J.: Magicmix: Semantic mixing with diffusion models. arXiv:2210.16056 (2022), <https://magicmix.github.io/> [4](#), [11](#), [12](#), [22](#)
36. Liu, L., Ren, Y., Lin, Z., Zhao, Z.: Pseudo numerical methods for diffusion models on manifolds. In: Proceedings of International Conference on Learning Representations (ICLR) (2022) [3](#)
37. Liu, N., Li, S., Du, Y., Torralba, A., Tenenbaum, J.B.: Compositional visual generation with composable diffusion models. In: Proceedings of the European Conference Computer Vision (ECCV). pp. 423–439 (2022) [2](#), [4](#)
38. Maher, M.L.: Evaluating creativity in humans, computers, and collectively intelligent systems. In: Proceedings of the 1st DESIRE Network Conference on Creativity and Innovation in Design. pp. 22–28 (2010) [2](#), [4](#)
39. Nobari, A.H., Chen, W., Ahmed, F.: Range-constrained generative adversarial network: Design synthesis under constraints using conditional generative adversarial networks. *Journal of Mechanical Design* **144**(2), 021708 (2021) [4](#)
40. Nobari, A.H., Rashad, M.F., Ahmed, F.: Creativegan: Editing generative adversarial networks for creative design synthesis. In: Proceedings of ASME International Design Engineering Technical Conferences and Computers and Information in Engineering Conference (2021) [4](#)
41. Orgad, H., Kawar, B., Belinkov, Y.: Editing implicit assumptions in text-to-image diffusion models. In: Proceedings of the IEEE/CVF International Conference on Computer Vision (ICCV). pp. 7053–7061 (2023) [4](#)
42. Park, D.H., Azadi, S., Liu, X., Darrell, T., Rohrbach, A.: Benchmark for compositional text-to-image synthesis. In: Proceedings of the Advances in Neural Information Processing Systems (NeurIPS) (2021) [4](#)
43. Radford, A., Kim, J.W., Hallacy, C., Ramesh, A., Goh, G., Agarwal, S., Sastry, G., Askell, A., Mishkin, P., Clark, J., et al.: Learning transferable visual models from natural language supervision. In: Proceedings of International Conference on Machine Learning (ICML). pp. 8748–8763 (2021) [2](#), [3](#), [9](#)
44. Ramesh, A., Dhariwal, P., Nichol, A., Chu, C., Chen, M.: Hierarchical text-conditional image generation with clip latents. In: arXiv:2204.06125 (2022) [2](#), [3](#), [5](#), [10](#), [11](#), [13](#), [24](#)
45. Ren, J., Luo, J., Zhao, Y., Krishna, K., Saleh, M., Lakshminarayanan, B., Liu, P.J.: Out-of-distribution detection and selective generation for conditional language models. In: Proceedings of International Conference on Learning Representations (ICLR) (2023) [4](#)
46. Rombach, R., Blattmann, A., Lorenz, D., Esser, P., Ommer, B.: High-resolution image synthesis with latent diffusion models. In: Proceedings of the IEEE/CVF Conference on Computer Vision and Pattern Recognition (CVPR). pp. 10684–10695 (2022) [1](#), [2](#), [3](#), [5](#), [9](#), [10](#), [11](#), [13](#), [24](#)
47. Ruiz, N., Li, Y., Jampani, V., Pritch, Y., Rubinstein, M., Aberman, K.: Dreambooth: Fine tuning text-to-image diffusion models for subject-driven generation. In: Proceedings of the Advances in Neural Information Processing Systems (NeurIPS) (2022) [4](#)

48. Russakovsky, O., Deng, J., Su, H., Krause, J., Satheesh, S., Ma, S., Huang, Z., Karpathy, A., Khosla, A., Bernstein, M., Berg, A.C., Fei-Fei, L.: Imagenet large scale visual recognition challenge. *International Journal of Computer Vision (IJCV)* **115**(3), 211–252 (2015) [3](#), [9](#), [10](#), [12](#)
49. Saharia, C., Chan, W., Saxena, S., Li, L., Whang, J., Denton, E., Ghasemipour, S.K.S., Ayan, B.K., Mahdavi, S.S., Gontijo-Lopes, R., Salimans, T., Ho, J., Fleet, D.J., Norouzi, M.: Photorealistic text-to-image diffusion models with deep language understanding. In: *Proceedings of the Advances in Neural Information Processing Systems (NeurIPS)* (2022) [5](#)
50. Schuhmann, C., Beaumont, R., Vencu, R., Gordon, C., Wightman, R., Cherti, M., Coombes, T., Katta, A., Mullis, C., Wortsman, M., et al.: Laion-5b: An open large-scale dataset for training next generation image-text models. In: *Proceedings of Advances in Neural Information Processing Systems (NeurIPS): Datasets and Benchmarks Track*. pp. 25278–25294 (2022) [10](#), [11](#)
51. Shen, X., Liu, F., Dong, H., Lian, Q., Chen, Z., Zhang, T.: Weakly supervised disentangled generative causal representation learning. *Journal of Machine Learning Research* **23**, 1–55 (2022) [4](#)
52. Shen, Z., Liu, J., He, Y., Zhang, X., Xu, R., Yu, H., Cui, P.: Towards out-of-distribution generalization: A survey. *arXiv preprint arXiv:2108.13624* (2021) [4](#)
53. Song, Y., Dhariwal, P., Chen, M., Sutskever, I.: Consistency models. In: *Proceedings of International Conference on Machine Learning (ICML)* (2023) [3](#)
54. Träuble, F., Creager, E., Kilbertus, N., Locatello, F., Dittadi, A., Goyal, A., Schölkopf, B., Bauer, S.: On disentangled representations learned from correlated data. In: *Proceedings of International Conference on Machine Learning (ICML)*. pp. 10401–10412 (2021) [4](#)
55. Wang, R., Que, G., Chen, S., Li, X., Li, J., Yang, J.: Creative birds: Self-supervised single-view 3d style transfer. In: *Proceedings of the IEEE/CVF International Conference on Computer Vision (ICCV)*. pp. 8775–8784 (2023) [4](#)
56. Wu, X., Hao, Y., Sun, K., Chen, Y., Zhu, F., Zhao, R., Li, H.: Human preference score v2: A solid benchmark for evaluating human preferences of text-to-image synthesis. *arXiv preprint arXiv:2306.09341* (2023) [3](#), [10](#), [12](#), [13](#)
57. Xu, R., Zhang, X., Shen, Z., Zhang, T., Cui, P.: A theoretical analysis on independence-driven importance weighting for covariate-shift generalization. In: *Proceedings of International Conference on Machine Learning (ICML)*. pp. 24803–24829 (2022) [4](#)
58. Ye, N., Li, K., Bai, H., Yu, R., Hong, L., Zhou, F., Li, Z., Zhu, J.: Ood-bench: Quantifying and understanding two dimensions of out-of-distribution generalization. In: *Proceedings of the IEEE/CVF Conference on Computer Vision and Pattern Recognition (CVPR)*. pp. 7947–7958 (2022) [4](#)
59. Yu, J., Xu, Y., Koh, J.Y., Luong, T., Baid, G., Wang, Z., Vasudevan, V., Ku, A., Yang, Y., Ayan, B.K., Hutchinson, B., Han, W., Parekh, Z., Li, X., Zhang, H., Baldrige, J., Wu, Y.: Scaling autoregressive models for content-rich text-to-image generation. *Transactions on Machine Learning Research* (2022) [3](#)
60. Zhang, Y., Zhou, D., Hooi, B., Wang, K., Feng, J.: Expanding small-scale datasets with guided imagination. In: *Proceedings of Advances in Neural Information Processing Systems* (2023) [4](#), [11](#)
61. Zhao, W., Bai, L., Rao, Y., Zhou, J., Lu, J.: Unipc: A unified predictor-corrector framework for fast sampling of diffusion models. In: *Proceedings of Advances in Neural Information Processing Systems (NeurIPS)* (2023) [3](#)

62. Zhou, K., Yang, Y., Hospedales, T., Xiang, T.: Deep domain-adversarial image generation for domain generalisation. In: Proceedings of AAAI Conference on Artificial Intelligence (AAAI). vol. 34, pp. 13025–13032 (2020) [4](#)
63. Zhou, K., Yang, Y., Hospedales, T., Xiang, T.: Learning to generate novel domains for domain generalization. In: Proceedings of European Conference Computer Vision (ECCV). pp. 561–578 (2020) [4](#)
64. Zhu, M., Pan, P., Chen, W., Yang, Y.: Dm-gan: Dynamic memory generative adversarial networks for text-to-image synthesis. In: Proceedings of the IEEE/CVF Conference on Computer Vision and Pattern Recognition (CVPR). pp. 5802–5810 (2019) [3](#)

A Learning a Neural Swapping Network

In this subsection, we learn a neural swapping network to generate the meaningful combinatorial object images with different styles. The swapping part in the subsection 3.1 is rewritten as follows:

Swapping their column vectors by learning a neural swapping vector,

$$E_f = E_1 \text{diag}(f) + E_2 \text{diag}(1 - f), \quad (9)$$

where $f = S(\text{cat}(E_1, E_2); \psi) \in \{0, 1\}^{w \times 1}$ is a neural swapping network from the concatenated embedding, $\text{cat}(E_1, E_2)$, to a binary output that consists of three convolutional layers and two fully connected layers with the parameter ψ . The architecture of the swapping network consists of three convolutional layers with a 3×3 kernel size, followed by two fully connected layers.

Training Loss. Using our BASS method in **Algorithm 1**, we can get the optimal combinatorial image $I_{\text{opt}}^{(p_1, p_2)}$, and then find its swapping vector $f_{\text{opt}}^{(p_1, p_2)}$. Based on the neural swapping network $f = S(\text{cat}(E_1, E_2); \psi)$ in Eq. 9 and the optimal swapping vector $f_{\text{opt}}^{(p_1, p_2)}$, the training loss is defined as:

$$L = \frac{1}{|\mathcal{P}|} \sum_{(p_1, p_2) \in \mathcal{P}} \|f_{\text{opt}}^{(p_1, p_2)} - S(\text{cat}(E_1, E_2); \psi)\|_2, \quad (10)$$

where \mathcal{P} is a set of the prompt pairs (p_1, p_2) corresponding to the text pairs (t_1, t_2) , and $|\mathcal{P}|$ represents the cardinality of the set \mathcal{P} . To ensure training stability, we employed the RMSprop [24] optimizer.

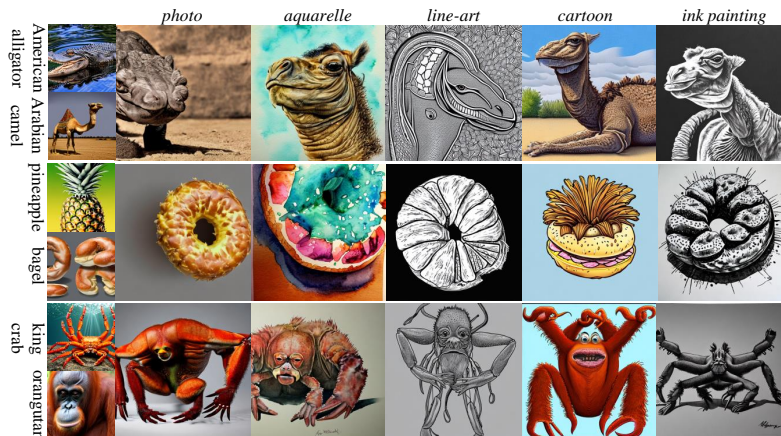


Fig. 10: Generalizations using four different styles including *aquarelle*, *line-art*, *cartoon*, and *ink painting*. It can observe that our results are still novel and surprising.

Generalizations using different styles. To evaluate the generalizations of our model, we expand its capabilities to four additional styles: *aquarelle*, *line-art*, *cartoon*, and *ink painting* for text-to-image generation. We achieve this without the need for excessive sampling and training. The results in Fig. 10, demonstrate

that our model maintains its impressive creativity by generating novel species across these different styles, such as (*orangutan*, *king crab*).

B More Comparison with Human Artworks

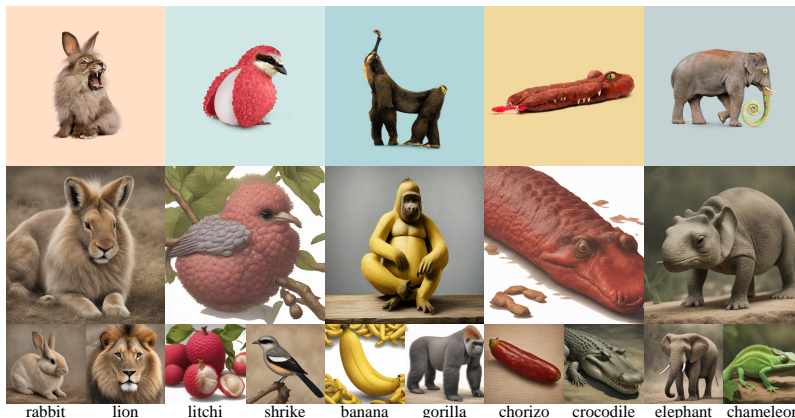


Fig. 11: More visualization results of artist comparison.

In this section, we provide more results of comparison with human artworks. In Figure 11, we present additional comparison results between our method

and images created by human artists. Similarly, the top row corresponds to images created by artists, the middle row to our results, and the bottom row to the prompts and corresponding image results used by both us and the artists. The results shown in the figure also illustrate that the fusion of our results tends to lean towards creating a new object that simultaneously incorporates features from both original prompts, rather than a simple fusion of two separate objects. Similarly, we conducted quantitative balanced-novelty calculations, as shown in Table 6. Our results outperform those of the artists in terms of balance.

Table 6: Quantitative comparisons with artist.

Model	Score	text-		image-	
		avg. sim.↓	balance↓	avg. sim.↓	balance↓
our BASS		0.351	0.037	0.647	0.016
artist		0.350	0.054	0.572	0.083

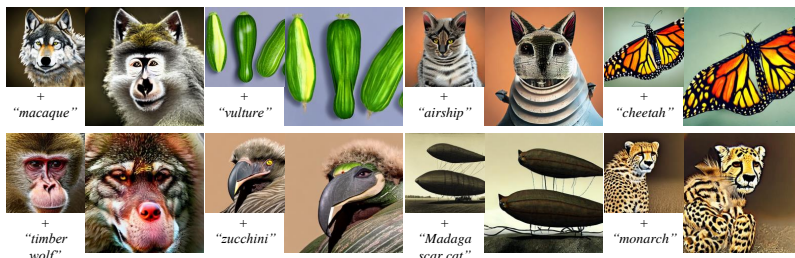


Fig. 12: Generalizations using unofficial code [13] of Magicmix with prompt-pairs in Figure 5.



Fig. 13: More visualization results of the User Study.

C More Comparisons with Magicmix

Here, we provide additional comparative results of our findings compared to those presented in Magicmix [35], except for Figure 6. As there is no open-source software available for Magicmix, we employed an unofficial implementation [13]. Utilizing the four text pairs depicted in Figure 5 to generate eight text-image pairs as inputs for Magicmix, the outcomes are illustrated in Figure 12. It is evident that our combined results significantly outperform those produced by Magicmix.

D User Study

In this section, we delve into a more comprehensive explanation of our user study. In addition to the five result categories showcased in Figure 5, we have included an additional set of five prompt-pair groups, as illustrated in Figure 13, to facilitate

* 1. Given the textual concepts of two different objects, please select which of the following options creatively combines the two objects in terms of novelty, surprise, and artistic value?

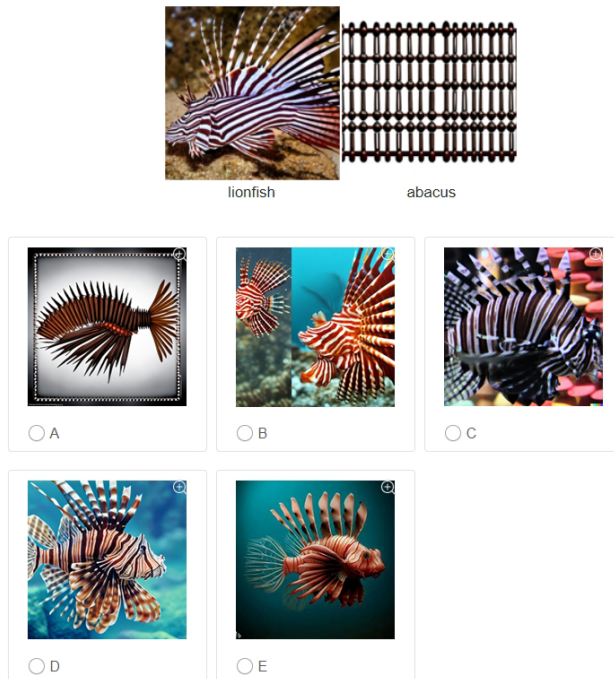


Fig. 14: interface of the User Study.

our User Study. Within these ten queries, we presented two prompts alongside their corresponding images. The interface of the User Study is depicted in Figure 14. We gathered responses from 106 participants who diligently completed our user study, and their decisions for each subject are presented in Table 7.

Furthermore, we present additional details of our user study comparing our results with those created by artists. We conducted the user study using 8 sets of images for comparison, with 5 sets from Figure 1 and the remaining 3 sets shown in Figure 15. The interface of the User Study is depicted in Figure 16. In this user study, we received 116 completed responses, and we display the results of each option in Table 8. From the results, it can be observed that, from the perspective of human preferences, our fused objects consistently outperform the subjectively created results of human artists.

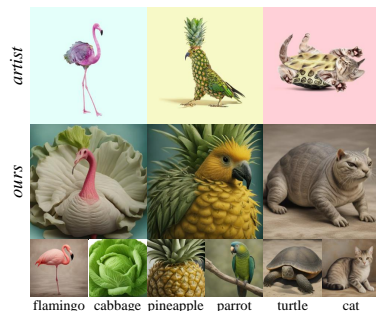
E Parameter Analysis

Here, we showcase sampled images generated with varying values of θ , $\bar{\alpha}$, and $\bar{\beta}$, as illustrated in Figures 17, 18, and 19.

In terms of the parameter θ 's setting, our evaluation method is adept at selecting the most creative images from diverse distributions. This is made

Table 7: The proportion of each option in each question in the User Study.

prompt-pairs	A(our BASS)	B(SD2 [46]-baseline)	C(DALLE-2 [44])	D(ERNIE-ViLG2 [18])	E(Bing)
lionfish and abacus	45.28%	13.21%	10.38%	18.87%	12.26%
lobster and sea slug	62.26%	12.26%	12.26%	3.77%	9.43%
kangaroo and pears	64.15%	20.75%	5.66%	4.72%	4.72%
sunflower and orange	75.47%	15.09%	1.89%	2.83%	4.72%
macaque and timber wolf	75.47%	2.83%	2.83%	3.77%	15.09%
Australian terrier and tiger	51.89%	12.26%	1.89%	3.77%	30.19%
toucan and bathing cap	27.36%	3.77%	4.72%	2.83%	61.32%
zucchini and vulture	85.85%	0.94%	1.89%	1.89%	9.43%
jackfruit and thresher	79.25%	0.94%	3.77%	1.89%	14.15%
CD player and beer glass	53.77%	10.38%	10.38%	1.89%	23.58%

**Fig. 15:** More visualization results of artist comparison User Study.**Table 8:** The proportion of each option in each question in the artist comparison User Study.

prompt-pairs	A(our BASS)	B(artist)
frog and broccoli	65.38%	34.62%
eagle and cauliflower	68.64%	31.54%
owl and tiger	80.00%	20.00%
strawberry and dinosaur	71.54%	28.46%
giraffe and snail	54.62%	45.38%
turtle and cat	68.46%	31.54%
pineapple and parrot	73.85%	26.15%
flamingo and cabbage	74.62%	25.38%

possible by dynamically determining $\bar{\alpha}$ and $\bar{\beta}$ based on these different distributions. However, this dynamic determination process is time-consuming. To streamline and expedite this process, we introduce a strict threshold for θ before proceeding to the overall ranking. This threshold effectively screens out images that require no further creative evaluation, as they exhibit evident biases. These biases, at this initial stage, contribute to the absence of creativity in the images, rendering them akin to straightforward outputs stemming directly from the prompt they are biased towards. We provide some illustrative results in Figure 17.

When $\bar{\beta}$ is set at 0.1, an increase in $\bar{\alpha}$ beyond our predefined value results in a biased image favoring one of the prompt pairs. Conversely, if $\bar{\alpha}$ falls below the predetermined threshold, the sampled image may appear unconventional due to the limited sampling space, as depicted in the shallow blue zone in Fig. 4. This is because the optimal sample tends to be biased for acceptability. Furthermore, when $\bar{\alpha}$ is held constant at 0.4, varying $\bar{\beta}$ can help validate the assertion that lower values of $\bar{\beta}$ result in increased urgency, whereas higher values lead to heightened confusion.

F Failure Examples

Here, we illustrate instances of unsuccessful model outputs. Some prompt-pairs, as depicted in Figure 20, prove challenging to generate novel and imaginative

* 1. Given the textual concepts of two different objects, please select which of the following options creatively combines the two objects in terms of novelty, surprise, and artistic value?

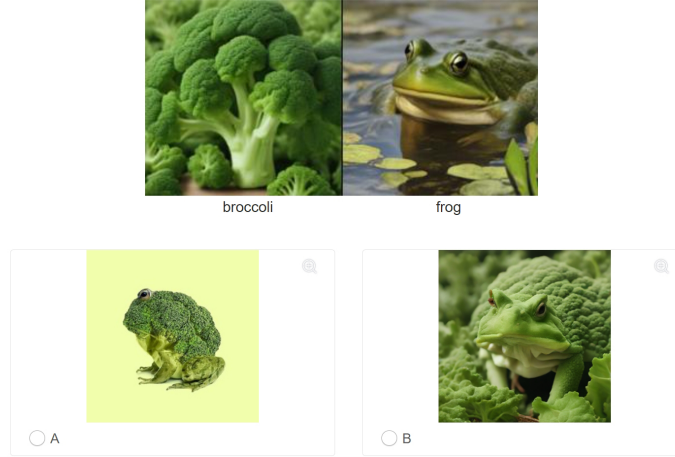


Fig. 16: interface of the artist comparison User Study.

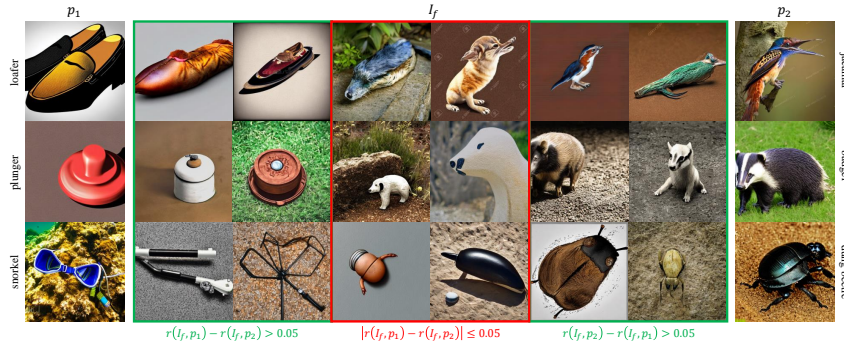


Fig. 17: Visualizations with different θ .

content. Even PickScore and HPS-v2 fail to produce satisfactory samples in such cases. While increasing the sample size may potentially address this issue, the likelihood of encountering this situation is exceptionally low, estimated at approximately 5%. Given our overall computing resources, we will refrain from excessive processing of these samples.

During the sampling stage, the primary reason for subpar samples is the inadequate configuration of hyperparameters α and β . Despite these values being established through consensus in our experiments, they tend to align with the distribution of majority classes, neglecting the minority classes. In our upcoming research, our focus will shift towards tailoring the distribution to the most creative samples across all categories and enhancing our model to reduce the occurrence of failed samples.

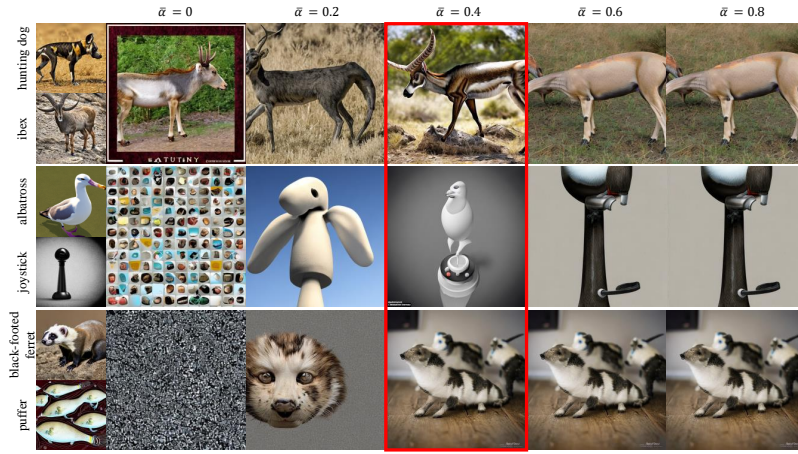


Fig. 18: Visualizations with different $\bar{\alpha}$ when $\bar{\beta} = 0.1$.



Fig. 19: Visualizations with different $\bar{\beta}$ when $\bar{\alpha} = 0.4$.

G More Visual Results

In the following section, we delve into supplementary findings. Figure 21 illustrates a comprehensive comparison of our results with those of other T2I models. Additionally, Figure 22 showcases a collection of visually captivating and groundbreaking results.



Fig. 20: Failure samples in evaluation stage.

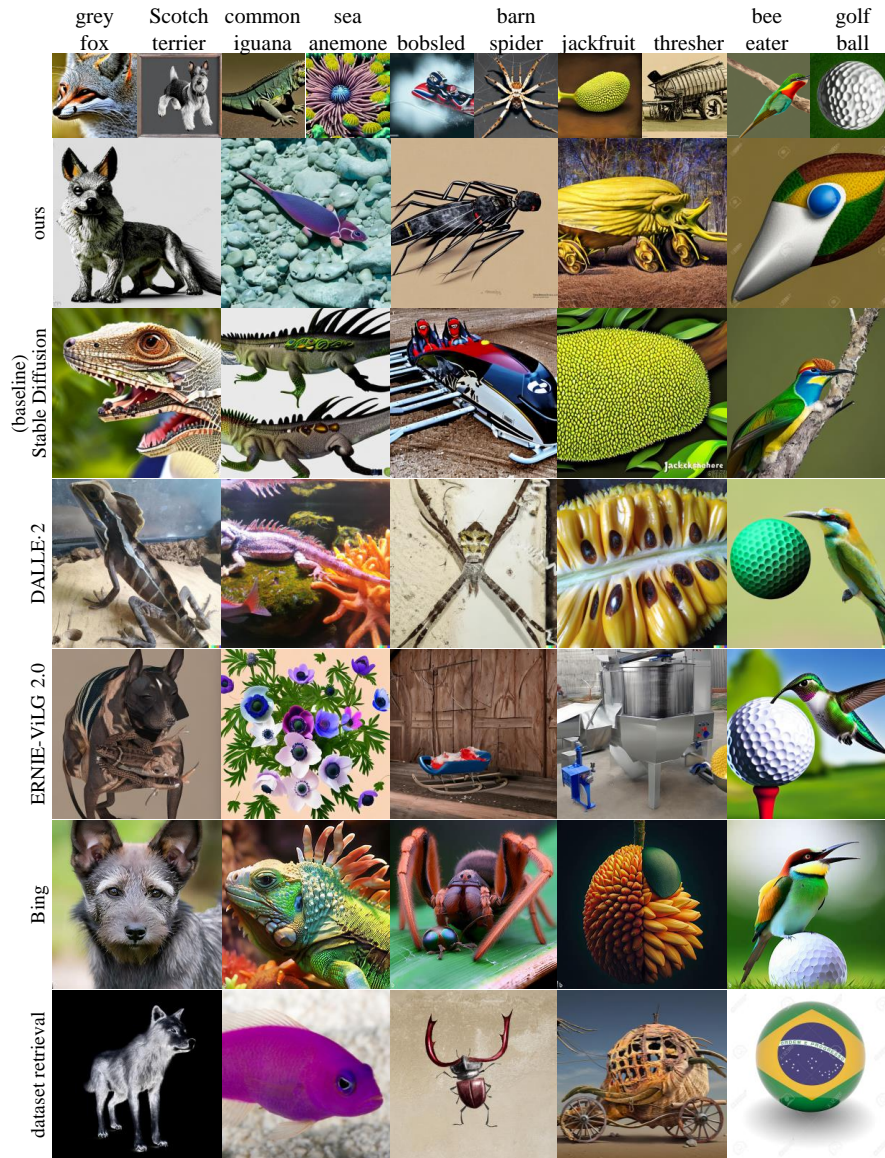


Fig. 21: More visual results and comparison to other T2I models using the prompts: "Hybird of [prompt1] and [prompt2]".

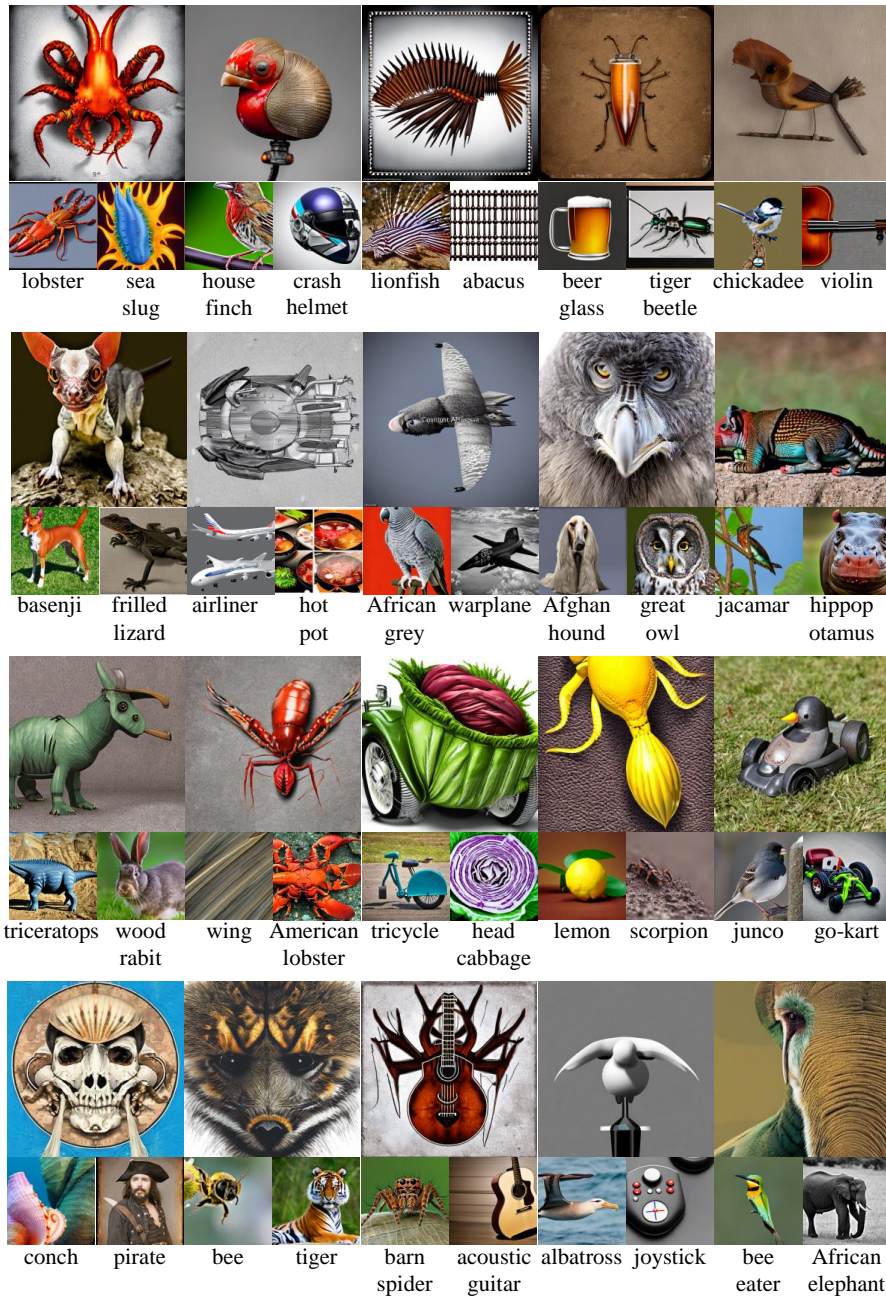


Fig. 22: More visual results.